

Liquation Phenomena in the Simulated Heat-Affected Zone of Alloy 718 after Multiple Postweld Heat Treatment Cycles

Delta-phase formation increases liquation cracking susceptibility

BY M. QIAN AND J. C. LIPPOLD

ABSTRACT. Long-term isothermal solution heat treatments were conducted to simulate multiple weld repair/postweld heat treatment cycles in Alloy 718 wrought plate. These heat treatments resulted in extensive precipitation of needle- and plate-shaped δ phase in the γ -nickel matrix. δ -phase accumulation represents the principal metallurgical damage from simulated multiple repair/postweld heat treatment cycles in Alloy 718. Grain size did not increase during this exposure due to the grain boundary pinning effect of the δ phase. Simulated weld heat-affected zone thermal cycles resulted in a variety of microstructural changes to the heat treated material, including δ -phase dissolution-promoted liquation, boron carbide constitutional liquation, and segregation-induced grain boundary liquation. The effect of these liquation phenomena on the weldability degradation of Alloy 718 is discussed.

Introduction

Weld repair of aircraft gas turbine engine components has become increasingly prevalent as a means of extending engine life and reducing the costs associated with component replacement. As part of the repair welding process, the precipitation-hardened superalloys must undergo postweld heat treatment (PWHT) to restore their mechanical properties. Because components are subject to multiple repairs over their lifetimes, they will also be exposed to multiple cycles of PWHT. It has been observed that the weldability of some superalloys degrades after an accumulation of repair/PWHT cycles (Refs. 1–5), making further repair difficult. Heat-affected zone (HAZ) liquation cracking is the root cause of this difficulty, which occurs in the partially melted region of the HAZ. Such cracking has been

shown to be associated with local or partial melting of grain boundaries, causing a short time high temperature grain boundary (GB) weakening (Ref. 6). Preliminary investigations on the effect of multiple PWHT cycles on repair weldability have been conducted for Alloy 718 (Refs. 2–5, 7). A direct result of the multiple PWHT is the accumulated, abundant δ -phase (Ni_3Nb , orthorhombic) precipitation in the nickel matrix, constituting the metallurgical “damage” that degrades the weldability of Alloy 718. The δ -phase dissolution during weld thermal cycles was reported to be a factor resulting in grain boundary liquation (Ref. 7) by promoting GB segregation of Nb, a melting point depressant (Ref. 1). The purpose of this paper is to elucidate the effect of liquation phenomena on the weldability degradation in the Alloy 718 due to multiple repair/PWHT cycles.

Experimental Procedure

The material used in this study was Alloy 718 in the form of wrought plate. The composition of this material, based upon an independent analysis, is shown in Table 1. The plate microstructure in the as-received condition is shown in Fig. 1. There are fine deformed grains surrounding the “normal” grains and some δ phase is present in the γ -nickel matrix. Simulation of multiple PWHT cycles was accomplished through metallurgical-equivalent long-term isothermal heat treatments. This technique had previously been shown to yield microstructures and properties

similar to those achieved through multiple thermal cycles for equivalent times (Ref. 6). A normal PWHT for Alloy 718 would be 954°C for 0.5–2 h. Two isothermal treatments were performed to simulate multiple PWHT cycles: 954°C/40 h and 954°C/100 h. The isothermal treatments were conducted in air in a box furnace with air cooling. Subsequently, Gleeble hot ductility specimens were machined from the bulk materials after heat treatment.

Gleeble hot ductility testing was conducted to evaluate and compare the susceptibility of Alloy 718 to HAZ liquation cracking in three different conditions: 1) as-received, 2) 954°C/40 h, and 3) 954°C/100 h. The specimens are 6.35 mm in diameter, 100 mm in length, taken longitudinally along the rolling direction in the plate. The hot ductility testing follows conventional procedures as have been reported previously (Refs. 2–7). A heating rate of 111°C/s, hold time at test temperature of 0.5 s, cooling rate of 43°C/s (for on-cooling tests), and stroke rate of 25 mm/s were used. All testing was conducted under an argon atmosphere. Figure 2 schematically shows the procedure for determining critical values of nil-strength temperature (NST), nil-ductility temperature (NDT), and ductility-recovery temperature (DRT). Initially, the nil-strength temperature (NST) was determined by heating the specimen under a small static load (approximate 10 kg) until failure occurred. On-heating hot ductility tests were conducted by heating samples to various test temperatures, and pulling them to failure at the stroke rate reported, until NDT was achieved. On-cooling tests were performed after heating to a peak temperature (T_p) between the NDT and NST, and then cooling to a desired temperature, and pulling to failure to identify the DRT.

Metallographic samples were examined using both an optical microscope and a Phillips XL-30 scanning electron microscope (SEM) equipped with an energy-dispersive spectrometer (EDS). Electrolytic etching with 10% aqueous chromic acid was generally used to reveal

KEY WORDS

Alloy 718
Weld Repair
 δ -Phase Precipitation
Boron Carbide Constitutional
Liquation
Liquation Cracking
Intergranular Fracture

M. QIAN and J. C. LIPPOLD are with the Welding and Joining Metallurgy Group at The Ohio State University, Columbus, Ohio.

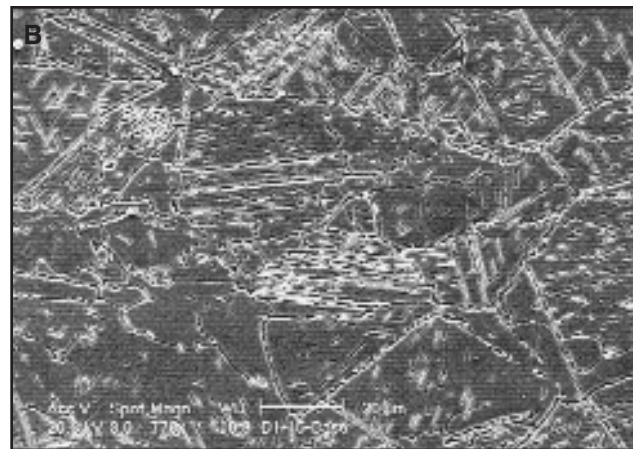


Fig. 1 — Microstructure of as-received Alloy 718 base metal: A — distribution of fine deformed grains at grain boundaries; B — short bar-shaped intra- and intergranular δ phase.

Table 1 — Chemical Composition of Alloy 718 Wrought Plate

Element	wt-%
Cr	18.42
Mn	0.09
Co	0.2
V	0.022
Al	0.5
C	0.033
Ti	1.03
B	0.0018
Mo	3.03
Si	0.1
Nb	5.04
S	0.0005
Fe	17.58
P	0.012
W	0.029
Mg	0.011
Cu	0.15
Ta	0.006
Ni	Balance

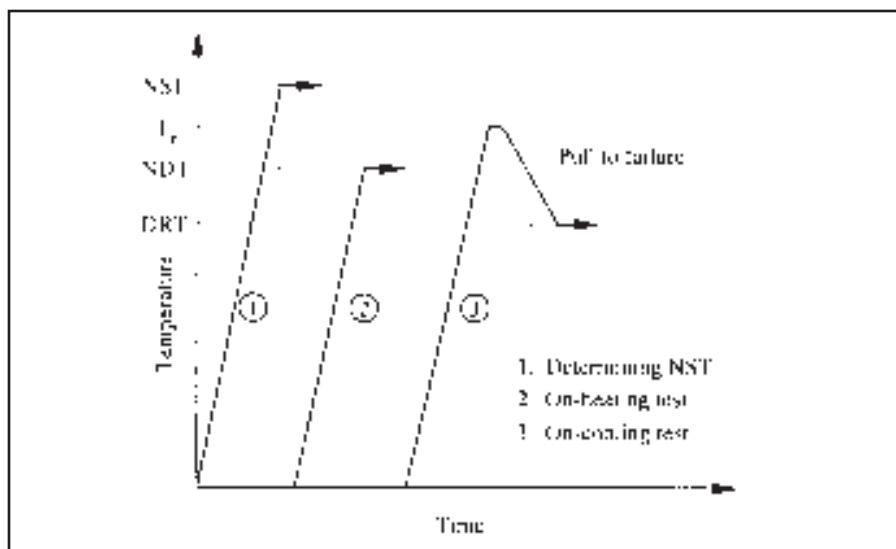


Fig. 2 — Schematic of Gleeble hot ductility test procedure.

Table 2 — The Effect of Heat Treatment on Grain Size of Alloy 718

HT Condition	Grain Size (d_f)
As-received	$79 \pm 40.6 \mu\text{m}$
954°C (1750°F)/40 h	$83 \pm 27 \mu\text{m}$
954°C (1750°F)/100 h	$83 \pm 31 \mu\text{m}$

microstructures of interest. Grain size was measured in Feret diameter (d_f), on digitally recorded optical images using *Image-Tool 2.0* (Ref. 8). Fracture morphology was evaluated on selected hot ductility samples by using SEM.

Results and Discussions

The principal microstructural feature in long-term isothermally treated Alloy

718 is the high fraction of precipitated δ phase relative to that of the as-received material. The as-received base metal had relatively little δ phase and the size of intra- and intergranular bar-shaped δ phase is comparable — Fig. 1. In contrast, the fraction of both intra- and intergranular (IG) δ phase in the long-term, isothermally treated material increased dramatically, as shown in Fig. 3. The intergranular δ phase becomes essentially continuous as a result of the long-term isothermal treatment, and some bar-shaped δ phase along twin boundaries also became continuous. The morphology of the intragranular δ phase appears as fine needles that intercrossed compactly — Fig. 3B. There was no evidence of gamma double-prime (γ'') observed in this structure since the heat treatment temperature is above the precipitation range for γ'' and none would be

expected to form upon rapid cooling to room temperature. In addition, the rapid formation of the δ phase depletes the matrix of niobium, further reducing the possibility of γ'' .

The grain size remained essentially constant after the long-term isothermal heat treatment at 954°C , as shown in Table 2. This is due to the pinning effect of the δ phase on grain boundaries. The bulky angular phases in the nickel matrix (Fig. 3B) are carbides that are distributed as stringers in the rolling direction of the wrought plate.

Gleeble hot ductility testing revealed HAZ liquation cracking susceptibility increases with the increase in hold time at 954°C , as determined by the liquation temperature range (LTR), which is the difference between NST and DRT (Table 3). Noticeably, the increase of LTR is consis-

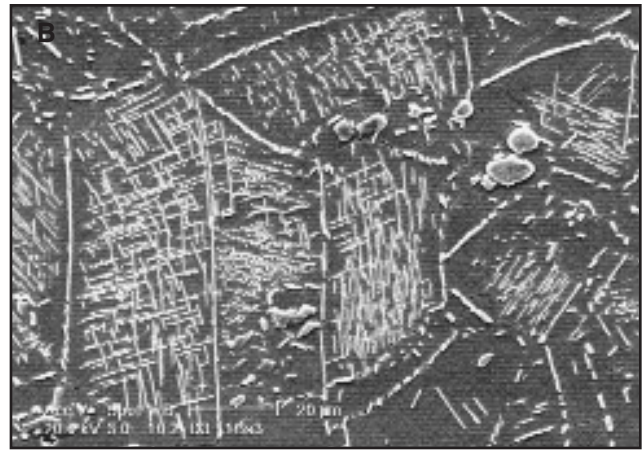
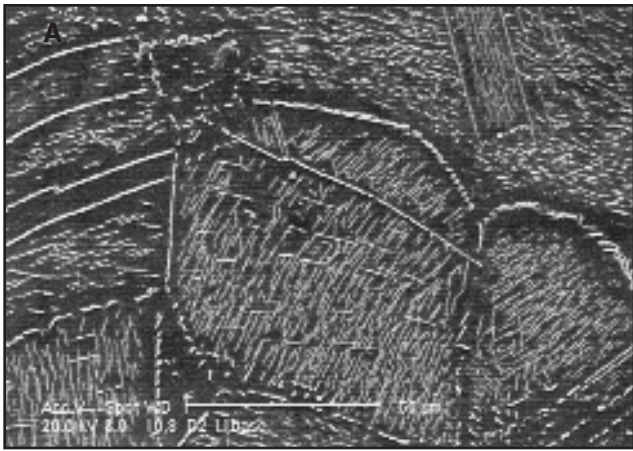


Fig. 3 — High fraction of needle-shaped intragranular and bulky continuous, intergranular δ phase from long-term isothermal treatment. A — 954°C/40 h; B — 954°C/100 h.

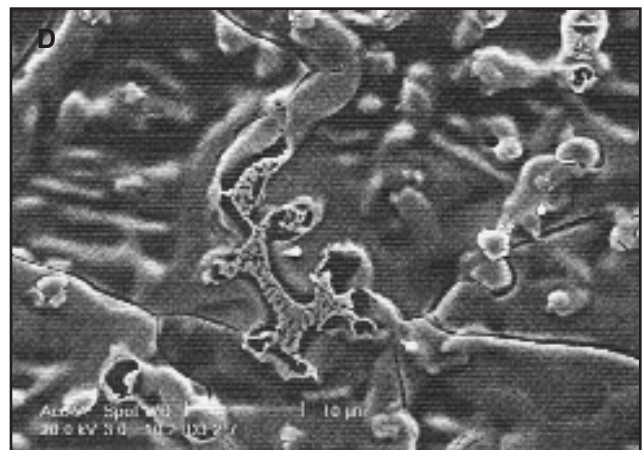
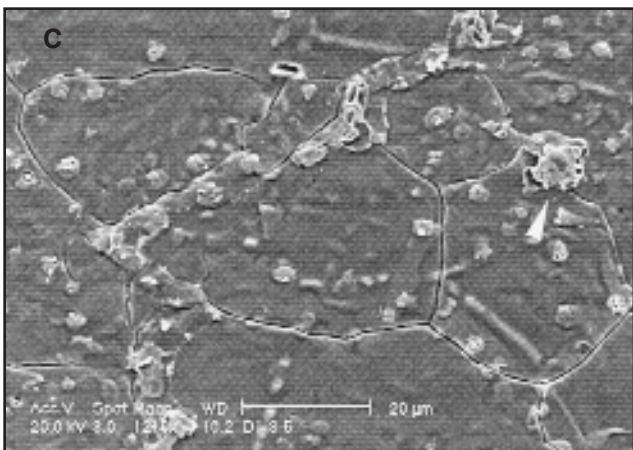
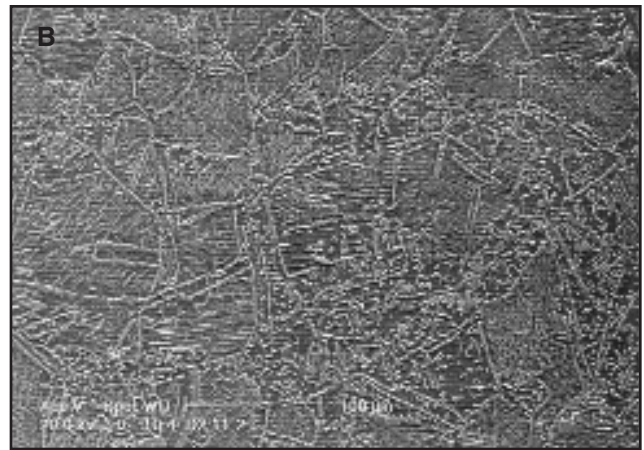
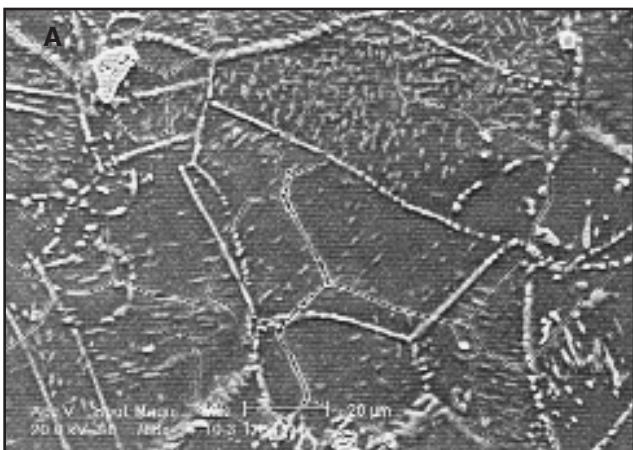


Fig. 4 — δ -phase dissolution during simulated HAZ thermal cycles in Alloy 718. A — δ -phase “thickening” at NDT of the as-received material; B — dissolving δ -phase network at NDT of 954°C/40 h treated material; C — δ phase “rounding” at NST of the as-received material (liquefied boron carbide is indicated); D — interconnected cluster of B- and Nb-rich eutectic constituents from dissolved δ -phase along grain boundaries at NST of 954°C/100 h-treated material.

tent with the density increase of δ phase as a function of hold time at 954°C.

Microstructural evaluation revealed that δ -phase dissolution-promoted liquation occurs during the on-heating thermal cycle and persists to the NST. δ phase has an orthorhombic structure with composi-

tion of Ni_3Nb . In Alloy 718, its precipitation temperature range is from 650 to 1050°C (Refs. 9, 10). δ phase will dissolve above the upper temperature limit. Upon dissolution, the surrounding γ -nickel matrix is enriched in Nb, both intra- and intergranularly depending on the δ -phase

distribution. Since Nb forms two eutectics with Ni as ($Ni+Ni_3Nb$) at 1282°C (23 wt-% Nb) and ($Ni_3Nb+Ni_6Nb_7$) at 1175°C (52 wt-% Nb), Nb acts as a melting point depressant element in Ni (Refs. 11, 12). With regard to Alloy 718, it is expected that the dissolution of δ phase will result

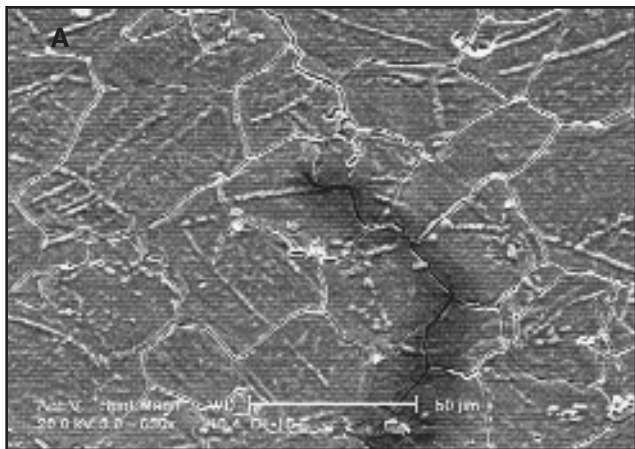


Fig. 5 — δ -phase dissolution gradient in DRT specimens. A — As-received; B — 954°C/100 h treated condition (arrows indicate eutectic constituents formed in the cores of original δ phase).

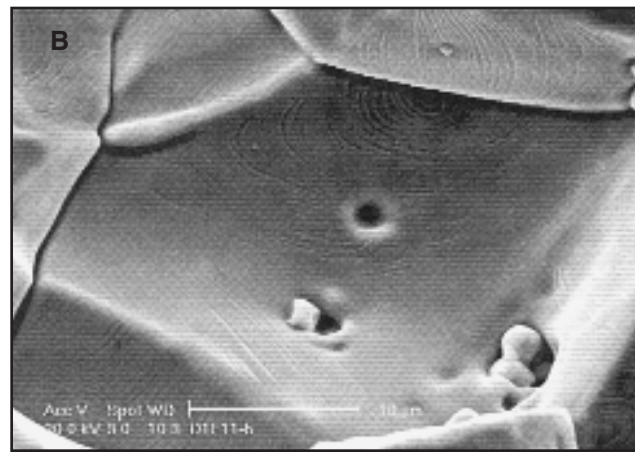
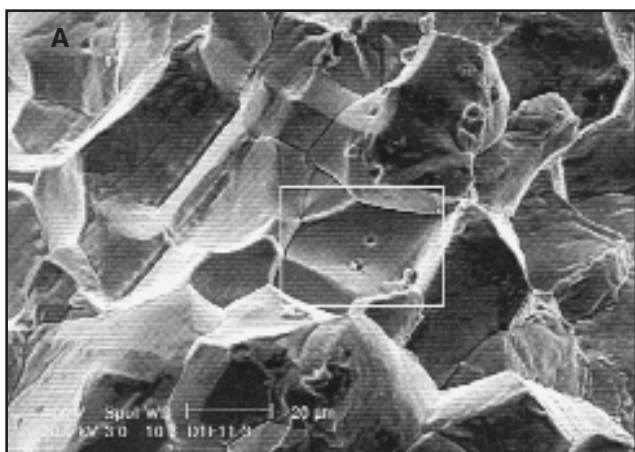


Fig. 6 — Fractography of NDT samples of as-received Alloy 718. A — Intergranular fracture; B — detail of Fig. 6A showing evidence of liquid films and liquated boron carbides.

Table 3 — Results of Gleeble Hot Ductility Testing for Alloy 718

HT Condition	NDT	NST	DRT	Peak temp (T_p)	LTR	T_p -DRT
As-received	1199°C	1274°C	1171°C	1240°C	103°C	69°C
954°C/40 h	1191°C	1272°C	1158°C	1240°C	114°C	82°C
954°C/100 h	1190°C	1276°C	1149°C	1240°C	127°C	91°C

in formation of Nb-rich eutectic constituents, as has been observed in the current research.

Figure 4 shows microstructural evidence of δ -phase dissolution and associated liquation. The dissolution of the δ phase results in Nb enrichment at the grain boundary that gives rise to the different etching characteristic of the boundary. The Nb-enriched boundary varied as a function of the peak temperature reached during the hot ductility test and is manifested microstructurally by different morphologies. At the NDT, the mi-

crostructure appears as δ -phase needle “thickening,” as shown in the as-received material — Fig. 4A. Note that the “holes” along the GBs are sites of eutectic, δ -phase dissolution products that have etched out of the structure. Fracture surface analysis in the SEM revealed additional details of the liquation process, including apparent constitutional liquation of boron carbides.

Typical intergranular features are shown in Fig. 6, where liquated particles and evidence of liquid films on the fracture surface can be seen. Note the angular

but slightly rounded particles and holes where particles have dropped out of the fracture surface — Fig. 6A and B. EDS analysis revealed that the particles are complex boron carbides containing Cr, Ti, and some Nb. The presence of round holes accommodating the rounded boron carbides suggests that boron carbide-related constitutional liquation has occurred along the GBs. Heating of the densely distributed δ phase in 954°C-treated samples to the NDT produced more extensive, dissolving δ phase networks — Fig. 4B. As the test temperature was raised to the NST, δ -phase dissolution became more pronounced. The once-thickened, intragranular δ -phase needles began “rounding” (Fig. 4C and D), indicating a more accelerated Nb dissolution rate. Some adjacent dissolved δ phase near or along GBs interconnected to form B- and Nb-rich eutectic constituents — Fig. 4D. These low-melting eutectic liquids along GBs will result in GB weaken-

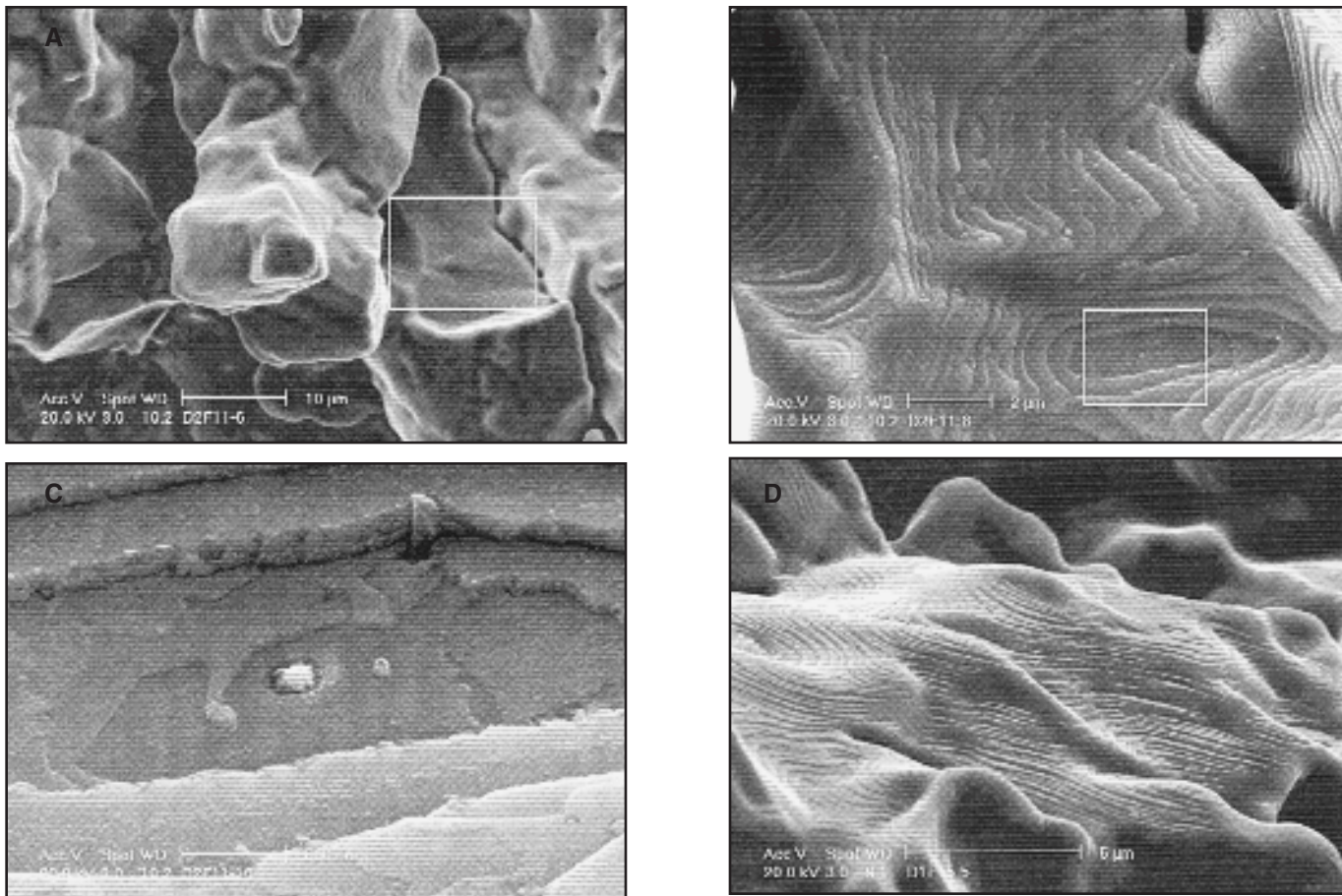


Fig. 7 — Fractography of 954°C/40 h-treated specimens. A — IG feature at NDT; B — detail of Fig. 7A showing terraced ripple pattern with particles dispersed at NDT; C — detail of the liquated boron carbide; D — terraced ripple pattern of liquid flow trace at DRT.

ing and potential failure (cracking) during the weld thermal cycle.

At the DRT, the microstructures of as-received 718 (Fig. 5A) did not change much compared with that of the NDT sample (Fig. 4A). However, the Nb dissolution is more extensive (Fig. 5B) than that at the NDT since this sample has been heated through the peak temperature (T_p) during the on-cooling test. It can also be observed that tiny but distinguishable eutectic constituents form in the center of the original δ phase — Fig. 5B. This is due to the Nb enrichment associated with the dissolved δ phase. The center has a higher concentration of Nb, while the periphery has a lower concentration of Nb. As the high concentration of Nb corresponds to the eutectic with a lower melting point (1175°C), liquation started preferentially at the center when temperatures became favorable.

Figure 7 shows intergranular fracture of the 954°C-treated samples, but with more liquid present than seen in Fig. 6 for the as-received material. There are more particles on these fracture surfaces and the flow pattern of the liquid films is much

more evident, appearing as terraced ripple patterns. At the center of concentric ripples, a liquated particle in a hole was identified as a Nb-rich boron carbide, as shown in Fig. 7B and C. Similar but smaller particles can also be differentiated in the same micrograph. The angular particle at the upper right has not liquated and was identified as TiC. More GB liquation associated with ripple patterns can be seen in Fig. 7D.

Figure 8 presents secondary electron (SE) and back-scattered-electron (BSE) micrographs that clearly show the morphology of boron carbides (lighter bulky phase) and MC carbides (dark phases), where boron carbide has apparently decomposed from its periphery. A similar case can be seen in Fig. 4C (arrow) and is probably due to constitutional liquation.

Based on the above results, it can be concluded that δ -phase dissolution-promoted liquation plays a major role in influencing the susceptibility to liquation cracking in Alloy 718 subjected to long-term heat treatments at 954°C. Segregation of B and Nb as well as other melting-point depressants also contribute to the

localized melting of the GB.

Interstitial elements, such as boron, are well known to have the propensity to segregate to GBs. Nb from the dissolution of δ phases could preferentially segregate to GB through either diffusion (Refs. 13, 14) or a segregation mechanism (Ref. 7), by which Nb could be swept by mobile GBs once the pinning effect of δ phase was reduced by dissolution.

Nb-containing boron carbide liquation also contributed to the Nb segregation to GBs, though this is expected to account for only a small fraction of the liquid present, since the fraction of boron carbides is much less than the δ phase. In addition, boron carbide liquation produces a low-melting eutectic, an extra low melting point constituent that further aggravates the liquation.

In summary, the effect of liquation phenomena on the susceptibility to liquation cracking of Alloy 718 that has been exposed to multiple PWHT cycles that result in a high fraction of δ phase can be explained as follows. As the number of weld repair cycles accumulates, δ -phase precipitation becomes more extensive. Upon re-

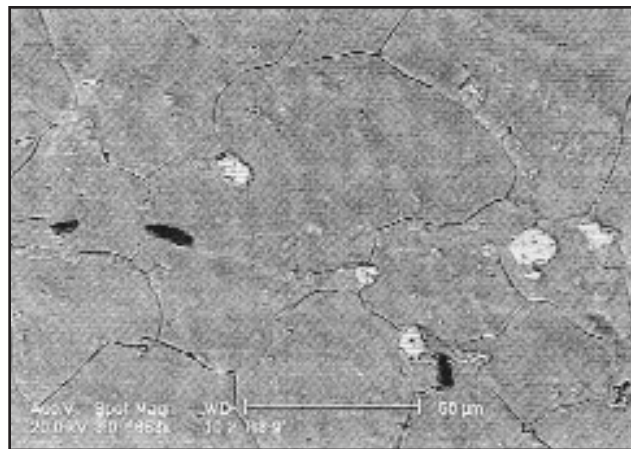
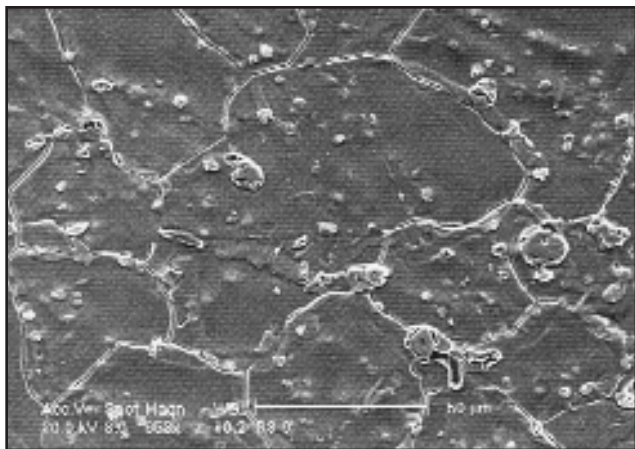


Fig. 8 — Morphology of boron carbides and MC carbides in a DRT specimen. A — SEM showing rounded δ phase and associated liquation; B — BSE image differentiating phases in the γ -nickel matrix.

heating in the weld HAZ, rapid δ -phase dissolution occurs. δ -phase dissolution-promoted liquation, possibly combined with boron carbide constitutional liquation, results in extensive grain boundary liquation that then leads to cracking if restraint levels are sufficient. This explains why the buildup of δ phase in Alloy 718 increases the susceptibility to HAZ liquation as the number of repair/PWHT cycles increases.

Conclusions

1) Simulated multiple PWHT cycles using equivalent long-term isothermal heat treatments (954°C/40–100 h) resulted in extensive precipitation of needle- and plate-shaped δ phase in the γ -nickel matrix, which is the major metallurgical change relative to the starting plate material. Grain size did not change appreciably during these heat treatments due to grain boundary pinning by the δ phase.

2) Gleeble hot ductility testing showed weldability (resistance to HAZ liquation cracking) of Alloy 718 degraded as a consequence of the simulated multiple PWHT cycles.

3) The degradation of weldability results from grain boundary liquation resulting primarily from the δ -phase dissolution and associated Nb enrichment of the grain boundary. Constitutional liquation of boron-rich carbides was also observed and may contribute to the grain boundary liquation.

Acknowledgment

The authors wish to thank Edison Welding Institute for supporting this research.

References

1. Chou, C. P., and Chao, C. H. 1988. Repair weldability studies of Alloy 718 using versatile vareststraint test. *Superalloys 1988*. Champion, Pa.: The Metallurgical Society/AIME, 18–22 Sept., pp. 785–794.
2. Lippold, J. C., Mehl, M., Lu, Q., Lin, W., and Kelly, T. J. 1996. Effect of composition, microstructure, and thermal treatment on the repair weldability of Alloy 718. *American Welding Society, 77th Annual AWS Convention Abstracts (USA)*. pp. 124–125.
3. Hooijmans, J. W., Lippold, J. C., and Lin, W. 1997. Effect of multiple postweld heat treatment on the weldability of Alloy 718. *Superalloys 718, 625, 706 and Various Derivatives*. Pittsburgh, Pa.: Minerals, Metals and Materials Society/AIME (USA). pp. 721–730.
4. Mehl, M. E., and Lippold, J. C. 1997. Effect of δ -phase precipitation on the repair weldability of Alloy 718. *Superalloys 718, 625, 706 and Various Derivatives*. Pittsburgh, Pa.: Minerals, Metals and Materials Society/AIME (USA), June 15–18, pp. 731–741.
5. Bowers, R. J., and Lippold, J. C. 1997. Effect of composition and heat treatment cycles on the repair weldability of Alloy 718. *Joining and Repair of Gas Turbine Components*. Indianapolis, Ind.: ASM International (USA), Sept., pp. 41–50.
6. Qian, M., 2001. An Investigation of the Repair Weldability of Waspaloy and Alloy 718. Ph.D. dissertation, The Ohio State University.
7. Lu, Q. 1999. HAZ Microstructural Evolution in Alloy 718 Multiple Repair and PWHT Cycles. Ph.D. dissertation, The Ohio State University.
8. *ImageTool* program developed at the University of Texas Health Science Center at San Antonio, Tex., and available from the Internet by anonymous FTP from <ftp://maxrad6.uthscsa.edu>.
9. Brown, E. E., and Muzyka, D. R. 1997. Nickel-iron alloys. *Superalloys II*. Ed. C. T. Sims, N. S. Stoloff, and W. C. Hagel. New York, N.Y.: John Wiley & Sons, pp.165–188.
10. Liu, W. C., Yao, M., Chen, Z. L., and Wang, S. G. 1999. Niobium segregation in Inconel 718. *Journal of Materials Science (UK)*. Vol. 34, No. 11, pp. 2583–86.
11. Duerden, I. J., and Hume-Rothery, W. 1966. The equilibrium diagram of the system niobium-nickel. *Journal of the Less-Common Metals*. Vol. 11, p. 381.
12. Zeng, K., Zeng, X. Z., and Jin, Z. P. 1992. A thermodynamic calculation of the Ni-Nb phase diagram. *Journal of Alloys and Compounds*. Vol. 179, pp. 177–185.
13. Boucher, C., Varela, D., Dadian, M., and Granjon, H. 1976. Hot cracking and recent progress in the weldability of the nickel alloys Inconel 718 and Waspaloy. *Revue de Metallurgie*. Vol. 73, pp. 817–831.
14. Vincent, R. 1985. Precipitation around welds in the nickel-base superalloy Inconel 718. *Acta Metallurgica*. Vol. 33, pp. 1205–16.

REPRINTS REPRINTS

To order custom reprints of
articles in
Welding Journal
Contact Denis Mulligan at
(800) 259-0470
FAX: (717) 481-7677
or via e-mail at
info@reprintdept.com

REPRINTS REPRINTS